

# TTHRESH: Tensor Compression for Multidimensional Visual Data

Rafael Ballester-Ripoll, *Member, IEEE*, Peter Lindstrom, *Senior Member, IEEE*,  
and Renato Pajarola, *Senior Member, IEEE*

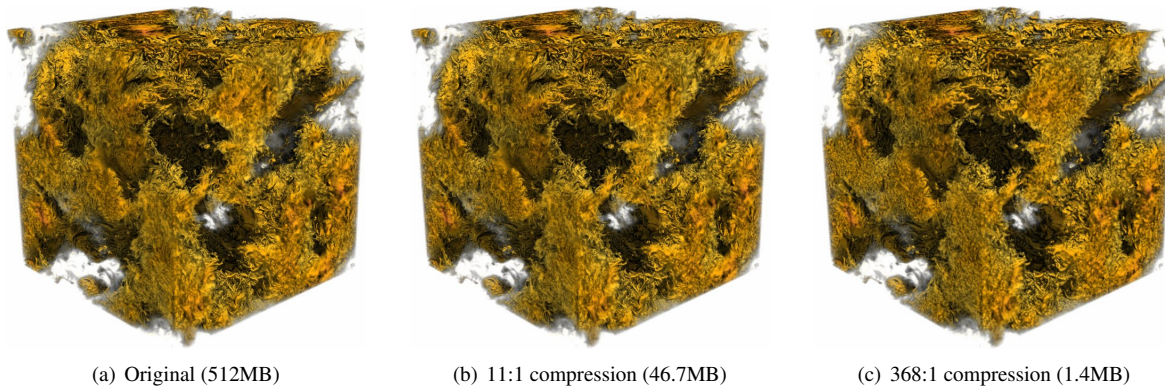


Fig. 1. (a) a  $512^3$  isotropic turbulence volume [1]; (b) visually identical compression result; (c) result after extreme compression.

**Abstract**—Memory and network bandwidth are decisive bottlenecks when handling high-resolution multidimensional data sets in visualization applications, and they increasingly demand suitable data compression strategies. We introduce a novel lossy compression algorithm for  $N$ -dimensional data over regular grids. It leverages the higher-order singular value decomposition (HOSVD), a generalization of the SVD to 3 and more dimensions, together with adaptive quantization, run-length and arithmetic coding to store the HOSVD transform coefficients' relative positions as sorted by their absolute magnitude. Our scheme degrades the data particularly smoothly and outperforms other state-of-the-art volume compressors at low-to-medium bit rates, as required in data archiving and management for visualization purposes. Further advantages of the proposed algorithm include extremely fine bit rate selection granularity, bounded resulting  $l^2$  error, and the ability to manipulate data at very small cost in the compression domain, for example to reconstruct subsampled or filtered-resampled versions of all (or selected parts) of the data set.

**Index Terms**—Transform-based compression, scientific visualization, higher-order singular value decomposition, Tucker model, tensor decompositions

## 1 INTRODUCTION

Most scientific and visual computing applications face heavy computational and data management challenges when handling large and/or complex data sets over Cartesian grids. Limitations in memory resources or available transmission throughput make it crucial to reduce and compress such data sets in an efficient manner. Lossy compression is often the prescribed strategy, since many applications admit a certain error (especially for higher bit depths and floating-point precision). If the compressed data set is to be used for subsequent computational analysis and/or to be fed as the initial state of a simulation routine, only small errors are typically tolerated. Conversely, if visualization and user exploration are to follow decompression, then higher error rates are acceptable; the method developed in this paper is mainly geared towards this case. Depending on the specific application, certain additional properties are sometimes desired. These may include fast support for random-access decompression, fine compression rate granularity, asymmetry (faster decompression than compression), bounded error,

support for arbitrary dimensionality, ease of parallelization, topological robustness, etc. These aspects make multidimensional compression a broad and challenging problem for which, unsurprisingly, no catch-all solution exists.

In this context, *tensor decompositions* and in particular the *Tucker model* are promising mathematical tools for higher-order compression and dimensionality reduction in the fields of graphics and visualization. 3D scalar field compression at the Tucker transform coefficients level was recently investigated [2], and it was concluded that coefficient thresholding outperforms earlier rank truncation-based approaches in terms of quality vs. compression ratio. This has motivated us to develop and introduce TTHRESH (from *Tucker thresholding*), a novel lossy compressor based on tensor decompositions. It is the first of its kind that supports arbitrary target accuracy via adaptive quantization. Previous related approaches fixed the number  $q$  of quantization bits per transform coefficient, and sometimes even the transform basis size (the *tensor ranks*). Instead, our method improves the compression ratio-accuracy trade-off curve by using thresholding granularity at the single-coefficient level combined with adaptive selection of  $q$ . While the reduction ratios we achieve for volume data sets and low error tolerances are comparable to other state-of-the-art compressors, we outperform them on the higher error ranges on which visualization tasks usually rely.

We have released an open-source C++ implementation of our algorithm<sup>1</sup>. It is primarily intended as a standalone command-line utility, although its main functions are also usable in a header-only library fashion.

- R. Ballester-Ripoll and R. Pajarola are with the Department of Informatics, University of Zürich, Switzerland.  
E-mails: {rballester, pajarola}@ifi.uzh.ch.
- Peter Lindstrom is with the Center for Applied Scientific Computing, Lawrence Livermore National Laboratory, USA.  
E-mail: pl@llnl.gov.

Manuscript received xx xxx. 201x; accepted xx xxx. 201x. Date of Publication xx xxx. 201x; date of current version xx xxx. 201x. For information on obtaining reprints of this article, please send e-mail to: reprints@ieee.org.  
Digital Object Identifier: xx.xxx/TVCG.201x.xxxxxx

<sup>1</sup> Available (LGPL-3.0) at <https://github.com/rballester/tthresh>.

## 2 RELATED WORK

### 2.1 3D Compression Algorithms

A number of lossy compression algorithms for scientific volume data sets have been proposed in the recent literature. For instance, ISABELA [3] focuses on spatio-temporal data with ample high-frequency components; it proceeds by sorting elements into a monotonic curve which is then fitted using B-splines. A more recent example of linearization strategy is SZ [4], which either predicts each coefficient using low-degree polynomials on preceding coefficients, or truncates it in its IEEE 754 binary representation. Some methods prioritize preserving specific properties of the data set, for example topological features [5] or bounded error over connected and coherent regions (e.g. SQ [6]). Vector quantization [7, 8] requires heuristics or greedy algorithms during compression, but is fast to decompress and thus suitable for compression-domain direct volume rendering; see also the survey [9]. In particular, [7] was defined within an octree multiresolution hierarchy for fast ray-casting in an interactive volume visualization application.

A popular and long-standing family of compression methods are the ones that exploit linear transforms, including well-known decompositions such as the Fourier and discrete cosine transforms and, since the 1990s, wavelets. They capitalize on carefully designed transform bases that aim to sparsify real-world signals as much as possible. VAPOR [10], for example, uses a flexible wavelet-based compression layer integrated into an interactive volume and flow exploration tool. ZFP [11] is a floating-point compressor using custom transform matrices that emphasizes fast random access and low error for e.g. storing snapshots and intermediate steps in a computational analysis/processing pipeline. ZFP offers a transparent interface for compressed C/C++ arrays and operates via fixed-rate encoding, although a variable-rate variant is also supported.

### 2.2 Compressors Based on Tensor Decomposition

Several transform-based compression algorithms have been recently defined that use data-dependent bases (the so-called *factor matrices*) instead of predefined ones. This is precisely the idea behind principal component analysis (PCA) as well as the Tucker decomposition. The Tucker model trades better transform-domain sparsity for the cost of storing its learned bases, which tends to be comparatively small for 3 or more dimensions. Some of the earliest Tucker-based compression approaches for visual data include [12], [13] and [14]. Progressive tensor rank reduction (the so-called *truncation*, see later sections) has been shown to reveal features and structural details at different scales in volume data [15]. Further recent efforts in the context of tensor compression include [2, 9, 16–18] for interactive volume rendering and visualization, [19] for 3D displays, [20] for integral histograms of images and volumes, and [21–24] for reflectance fields, among others. The large-scale renderer TAMRESH [17] resembles block-transform coding in that the input volume is partitioned in small multiresolution cubic bricks; each brick is then compressed as a separate HOSVD core. Recently, Tucker core hard thresholding combined with factor matrix quantization was shown [2] to yield better compression rate than slice-wise truncating the core. These points have motivated the compressor proposed here.

## 3 TUCKER/HOSVD COMPRESSION

Throughout this paper, tensors refer to multiarrays of dimension  $N \geq 1$ . We write vectors (tensors of dimension 1) in bold lowercase as in  $\mathbf{x} = (x_1, \dots, x_N)$ , matrices (tensors of dimension 2) in bold capitals such as  $\mathbf{U}$ , and general tensors as well as sets in calligraphic letters such as  $\mathcal{T}$ . We generally use the notation and definitions from [25]; in particular, rows and columns in matrices generalize to tensors as *fibers*. The  $n$ -th mode unfolding of a tensor  $\mathcal{T}$  arranges all  $n$ -mode fibers next to each other as columns of a wide matrix and is denoted as  $\mathbf{T}_{(n)}$ . The *tensor-times-matrix product* (TTM) contracts a tensor's  $n$ -mode fibers along a matrix's rows and is denoted as  $\mathcal{T} \times_n \mathbf{U}$ . We access tensors using bracket notation, so for instance  $\mathbf{U}[0, 0]$  is the top left element of

a matrix  $\mathbf{U}$ . We refer the reader to Kolda and Bader's survey [26] for more extensive details on basic tensor manipulation.

The root-mean-square error (RMSE) between a tensor of size  $I_1 \times \dots \times I_N$  and an approximation  $\tilde{\mathcal{T}}$  is defined as  $\|\mathcal{T} - \tilde{\mathcal{T}}\| / \sqrt{I_1 \dots I_N}$ , where  $\|\cdot\|$  denotes the Frobenius norm (i.e. the Euclidean norm of the flattened tensor). The error metric we use in our experiments (Sec. 6) is the peak signal-to-noise ratio (PSNR) in terms of the RMSE as follows:

$$\text{PSNR}(\mathcal{T}, \tilde{\mathcal{T}}) = 20 \cdot \log_{10} \left( \frac{\max\{\mathcal{T}\} - \min\{\mathcal{T}\}}{2 \cdot \text{RMSE}(\mathcal{T}, \tilde{\mathcal{T}})} \right). \quad (1)$$

### 3.1 The Tucker Model

The *full* Tucker decomposition [25, 27] writes each element  $x_1, \dots, x_N$  of a tensor  $\mathcal{T}$  exactly as:

$$\sum_{r_1, \dots, r_N=1}^{I_1, \dots, I_N} \mathcal{B}[r_1, \dots, r_N] \cdot \mathbf{U}^{(1)}[x_1, r_1] \dots \mathbf{U}^{(N)}[x_N, r_N] \quad (2)$$

or, in the more compact TTM notation,

$$\mathcal{T} = \mathcal{B} \times_1 \mathbf{U}^{(1)} \times_2 \dots \times_N \mathbf{U}^{(N)} \quad (3)$$

where each  $\mathbf{U}^{(n)}$  is a non-singular matrix of size  $I_n \times I_n$  and  $\mathcal{B}$  is a *core* tensor of coefficients with the *same* size as  $\mathcal{T}$ . See Fig. 2b) for an illustration of the full Tucker decomposition. The matrices  $\mathbf{U}^{(n)}$  are called *Tucker factors* (or *factor matrices*) and define a two-way transformation between  $\mathcal{T}$  and its core  $\mathcal{B}$ , whereby Eq. 3 is inverted as

$$\mathcal{B} = \mathcal{T} \times_1 \mathbf{U}^{(1)-1} \times_2 \dots \times_N \mathbf{U}^{(N)-1}. \quad (4)$$

The higher-order singular value decomposition (HOSVD) [25, 26] is an efficient procedure to construct orthogonal Tucker factors by setting each  $\mathbf{U}^{(n)}$  as the left singular vectors of the  $n$ -th mode unfolding matrix  $\mathbf{T}_{(n)}$ . In other words, it uses the PCA non-centered transformation matrix of the set of all fibers from  $\mathcal{T}$ , taken along the  $n$ -th mode. Furthermore, factor orthogonality implies that  $\|\mathcal{T}\| = \|\mathcal{B}\|$ . The Tucker format is flexible and readily applicable to any shape and dimensionality, and the HOSVD decomposition always exists.

### 3.2 Sparsifying Properties

Tucker-based compression algorithms exploit the fact that the HOSVD transform coefficients generated in  $\mathcal{B}$  tend to be quasi-sparse for typical real-world and simulated multidimensional signals. In addition, many transformations do not significantly affect the HOSVD. For example, if one permutes some slices of  $\mathcal{T}$  along one or more dimensions, its HOSVD will produce the same core  $\mathcal{B}$  and factors (with their corresponding rows permuted). Other possible transformations that can be encoded on a HOSVD-compressed data set without essentially affecting  $\mathcal{B}$  include spatially moving or stretching the data, padding it with zeros, upsampling it with multilinear interpolation, scaling by a constant (this will scale  $\mathcal{B}$ ), etc. Many usual data reduction approaches are guaranteed to actually improve HOSVD core sparsity, including downsampling, box-filtered decimation, convolving with any band-limited kernel, etc. For instance, a volume whose  $k$  last wavelet levels are zero can be represented using a Tucker core with  $8^k$  times fewer non-zero coefficients than otherwise needed.

The HOSVD decomposition decorrelates the data at all spatial scales, but does so without explicit space partitioning, i.e. avoiding tree-like structures or predefined multiresolution filter banks. The task of capturing correlation at multiple scales is thus undertaken by the different factor matrix columns. Nonetheless, the question of how to organize the coefficients in  $\mathcal{B}$  for effective compression is unclear *a priori*.

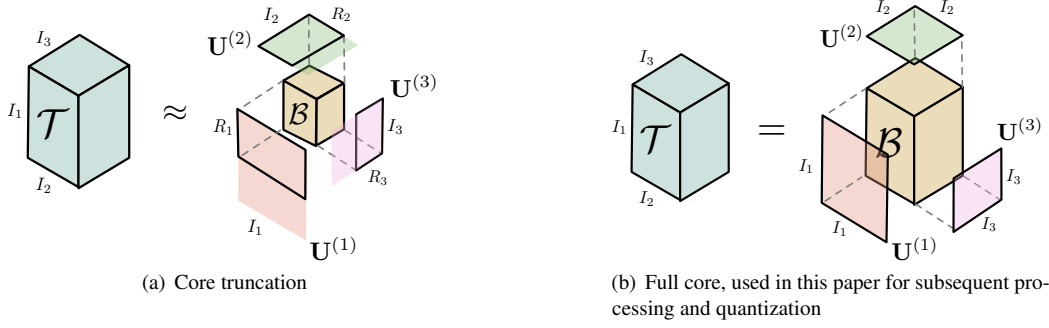


Fig. 2. Left: the Tucker rank truncation approach for 3D compression used in e.g. [14], [16], [17] and [18]. Right: the full core approach first considered in [2] and here extended into a full-fledged compressor with adaptive thresholding and coefficient quantization.

### 3.3 Core Truncation and Its Limitations

Conveniently, the HOSVD produces core (hyper-)slices that are non-increasing in norm. Let us consider the norm of each  $k$ -th slice of the Tucker core along the  $n$ -th dimension:

$$\sigma_k^{(n)} := \|\mathcal{T}[:, \dots, :, k, :, \dots, :]\|. \quad (5)$$

These norms have been proposed as *generalized singular values*, and they satisfy [25]:

$$\sigma_1^{(n)} \geq \sigma_2^{(n)} \geq \dots \geq \sigma_{I_n}^{(n)} \geq 0. \quad (6)$$

Furthermore, from the factor matrix orthogonality it follows that the mean squared error (MSE) induced by zeroing-out a core coefficient is proportional to its squared magnitude. These properties have been exploited in the past as the basis of several truncation-based HOSVD compression schemes [14], [16], [17], [18], whereby the least important trailing factor columns in each  $\mathbf{U}^{(n)}$  and the corresponding core slices in  $\mathcal{B}$  along each dimension are discarded to produce a compressed approximation. By doing so, only  $1 \leq R_n < I_n$  factor columns and core slices remain for each mode  $n$  (see Fig. 2a). The quantities  $R_1, \dots, R_N$  are known as *truncated Tucker ranks* and were used in those works for variable-detail compression and progressive reconstruction.

There are, however, two notable aspects that have not been pursued satisfactorily by these previous approaches. First, although the slice truncation idea is sound as motivated by Eq. 6, its granularity is very coarse. Elimination strategies on a coefficient-by-coefficient basis (rather than slice-by-slice) have the potential to significantly improve compression quality. Second, and regardless of the coefficient elimination method chosen, how to encode the surviving coefficients remains an open issue as well. Based on the roughly exponential growth of those coefficients (e.g. Fig. 3), [16] proposed a fixed-bit logarithmic quantization scheme: 1 bit for the coefficient sign and 8 or 16 for the logarithm of its absolute value. The authors realized the extreme importance of the first element  $\mathcal{B}[0, 0, 0]$  (the so-called *hot corner*); it often captures most of the signal's energy and  $\|\mathcal{B}[0, 0, 0]\| \approx \|\mathcal{T}\|$ . Hence this value was saved separately at 64-bit floating-point precision. This strategy was later replicated in other works [2, 17]. Nevertheless, a truly adaptive compression approach for the full-length HOSVD core has not been explored as of yet. The strategy we propose generalizes the thresholding-oriented analysis of [2] in that we sort and adaptively partition the full set of coefficients (Fig. 2b) according to their relative magnitude, and then encode each chunk at a variable quantization resolution. We give the full details in the following section.

## 4 PROPOSED ALGORITHM

Our compression pipeline consists of four main stages. First, the full non-truncated HOSVD is run on the  $N$ -dimensional data set to yield  $N$  orthogonal square factor matrices and an  $N$ -dimensional core of the same size as the original. Second, the core coefficients are sorted

and partitioned into chunks according to their absolute magnitude; coefficients within each  $q$ -th chunk are linearly quantized using  $q$  bits. We start with  $q = 0$  and stop adding chunks as soon as all coefficients have been quantized. Third, the positions of each chunk's coefficients along the unsorted core are expressed as a binary presence mask. These masks are compressed without loss using run-length encoding (RLE) followed by arithmetic coding. Last, the factor matrices are quantized column-wise, with each column using a different number of bins. All components are immediately streamed upon generation through the lossless compression algorithm ZLIB before written to disk. This pass provides a small extra compression, usually below 5%, mostly due to the distribution of coefficients. See Alg. 1 for a pseudocode of our compression pipeline; its individual building blocks are detailed next.

### 4.1 HOSVD Transform

We use the HOSVD as presented in Sec. 3 to compute orthogonal Tucker factors as the left singular vectors of unfolding matrices. In general one may directly compute these singular vectors from each unfolding  $\mathbf{B}_{(n)} = \mathbf{U}^{(n)} \cdot \boldsymbol{\Sigma}^{(n)} \cdot \mathbf{V}^{(n)T}$  in one run of any standard SVD algorithm. In volume compression, however, we usually have  $\mathbf{B}_{(n)} \in \mathbb{R}^{I \times J}$  with  $I \ll J$ . Since we do not need the  $J$  right singular vectors, in such cases it is much more efficient to compute first the matrix  $\hat{\mathbf{B}}_{(n)} = \mathbf{B}_{(n)} \cdot \mathbf{B}_{(n)}^T$  and then obtain all left singular vectors  $\mathbf{U}^{(n)}$  from the full eigenvalue decomposition  $\hat{\mathbf{B}}_{(n)} = \mathbf{U}^{(n)} \boldsymbol{\Lambda}^{(n)} \mathbf{U}^{(n)T}$ . Since  $\hat{\mathbf{B}}_{(n)}$  is a real symmetric matrix, its eigenvalue diagonalization always exists and we can use a more efficient specialized solver. The remaining rightmost part of the SVD follows from

$$\boldsymbol{\Sigma}^{(n)} \mathbf{V}^{(n)T} = (\mathbf{U}^{(n)})^{-1} \mathbf{B}_{(n)} = \mathbf{U}^{(n)T} \mathbf{B}_{(n)} \quad (7)$$

as the factor matrix  $\mathbf{U}^{(n)}$  is orthogonal. This process is undertaken  $N$  times. In the last iteration we reshape (fold)  $\boldsymbol{\Sigma}^{(N)} \cdot \mathbf{V}^{(N)T}$  back into an  $N$ -dimensional tensor, namely the core  $\mathcal{B}$ .

### 4.2 Adaptive Chunk Partitioning

Once the Tucker core  $\mathcal{B}$  is available we can turn to our adaptive quantization and encoding scheme. Note that, since no truncation was performed, we have not incurred yet any loss of accuracy other than floating-point roundoff error. Our goal now is to produce an approximate core  $\tilde{\mathcal{B}}$  so that each coefficient  $\tilde{\mathcal{B}}[x] \approx \mathcal{B}[x]$  contributes equally (on average) to the overall final desired mean squared error  $\epsilon$ . More specifically, we will sort and greedily split up the coefficients into chunks so that no chunk's MSE surpasses the target  $\epsilon$ . Each chunk is linearly quantized using a certain number of bits  $q$ . Let us consider the array  $s$  of core coefficients in absolute value, sorted in ascending order. We have observed (Fig. 3) that its elements generally grow at a much faster rate the later they appear in the magnitude curve. If we were to keep  $q$  constant as we move towards the larger elements, the chunk sizes would need to be dramatically reduced in order to keep their overall errors uniform. Having many small chunks is clearly

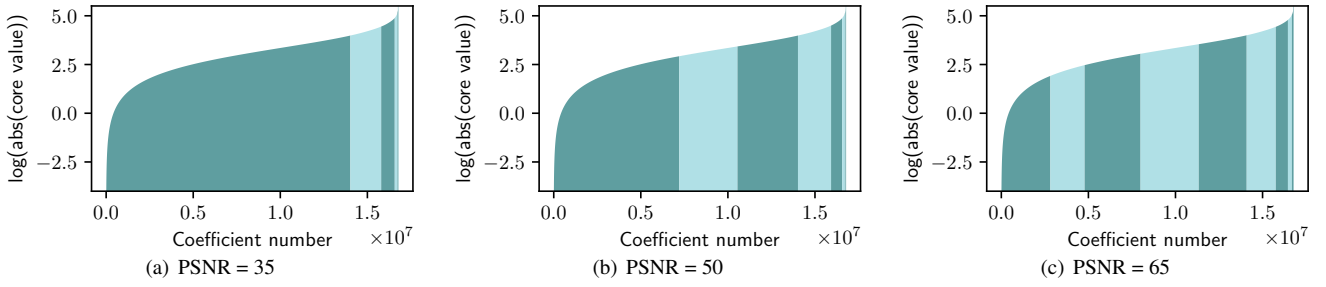


Fig. 3. Resulting adaptive chunk sizes along the Foot's sorted core curve at three target PSNR levels. In each plot the leftmost chunk is zeroed-out, while remaining chunks use an increasingly large number  $q$  of quantization bins.

**Algorithm 1** Compress an  $N$ -dimensional tensor  $\mathcal{T}$  of size  $I_1 \times \dots \times I_N$  at a prescribed mean squared error  $\epsilon$  using TTHRESH.

```

1:  $\mathcal{B} := \mathcal{T}$ 
2: for  $n = 1, \dots, N$  do
3:   {HOSVD transform}
4:    $\mathbf{B}_{(n)} := \text{unfold}(\mathcal{B}, n)$  {Size  $I_n \times (I_1 \cdots \hat{I}_n \cdots I_N)$ }
5:    $\hat{\mathbf{B}}_{(n)} := \mathbf{B}_{(n)} \cdot \mathbf{B}_{(n)}^T$  {Symmetric matrix of size  $I_n \times I_n$ }
6:    $\mathbf{\Lambda}^{(n)}, \mathbf{U}^{(n)} = \text{eig}(\hat{\mathbf{B}}_{(n)})$  {Full decomposition; eigenvalues  $\mathbf{\Lambda}^{(n)}$  in non-increasing order}
7:    $\mathbf{B}_{(n)} := \mathbf{U}^{(n)T} \cdot \mathbf{B}_{(n)}$  {Right part  $\mathbf{\Sigma} \cdot \mathbf{V}^T$  of the SVD}
8:    $\mathcal{B} := \text{fold}(\mathbf{B}_{(n)})$  {Back to original size}
9: end for
10: { $\mathcal{B}$  is now the HOSVD core, and  $\mathbf{U}^{(1)}, \dots, \mathbf{U}^{(N)}$  its factors}
11:  $\mathbf{a} := \text{flatten}(\mathcal{B})$ 
12:  $\mathbf{s} := \text{sort}(\text{abs}(\mathbf{a}))$  {Non-decreasing order}
13:  $\mathbf{m} := \text{argsort}(\text{abs}(\mathbf{a}))$  {Indices that map back to the original ordering, i.e.  $\mathbf{s}[\mathbf{m}[i]] = \text{abs}(\mathbf{a}[i])$ }
14:  $i_0 := 1$  {First threshold}
15:  $\mathcal{M} := \{1, \dots, I_1 \cdots I_N\}$  {Mask to record coefficients that have not been saved yet}
16: for  $q = 0, \dots, 63$  do
17:   Find the largest  $1 \leq i_{q+1} \leq I_1 \cdots I_N + 1$  such that

```

$$\frac{\text{error}(\mathbf{s}[i_q], \dots, \mathbf{s}[i_{q+1}])}{i_{q+1} - 1 - i_q} \leq \epsilon$$

```

    where the error( $\mathbf{u}$ ) is  $\|\mathbf{u} - \text{dequant}(\text{quant}(\mathbf{u}, q), q)\|^2$ 
18:    $\mathbf{c} := (0, \dots, 0)$  {Presence bits:  $I_1 \cdots I_N$  zeros}
19:    $\mathcal{M}^* := \mathcal{M}$ 
20:   for each  $1 \leq j \leq I_1 \cdots I_N$  such that  $i_q \leq \mathbf{m}(j) \leq i_{q+1}$  do
21:     Save quant( $\mathbf{a}[j], q$ )
22:      $\mathbf{c}[j] := 1$  {Mark as saved}
23:      $\mathcal{M}^* := \mathcal{M}^* \setminus j$ 
24:   end for
25:   Save arithmeticCoding(RLE( $\mathbf{c}[\mathcal{M}^*]$ ))
26:    $\mathcal{M} := \mathcal{M}^*$ 
27:   if  $\mathcal{M} = \emptyset$  then
28:     Exit loop {The whole core has been encoded}
29:   end if
30: end for
31: if  $\mathcal{M} \neq \emptyset$  then
32:   Save remaining coefficients in  $\mathcal{M}$  verbatim with 64-bit floating point precision
33: end if
34: for  $n = 1, \dots, N$  do
35:   for  $j = 1, \dots, I_n$  do
36:     Save quant( $\mathbf{U}^{(n)}[:, j], q_j^{(n)}$ ) { $q_j^{(n)}$  as in Eq. 9}
37:   end for
38: end for

```

undesirable since they incur large overhead, namely we need their respective minimum/maximum bounds plus their presence masks (see next subsection). To balance this, we conclude a chunk as soon as its average error reaches the target  $\epsilon$ , increase  $q$  by 1, and move on to the next coefficients. The extra bit halves the average per-coefficient error and thus adaptively counteracts the roughly exponential increase in magnitude as we progress along the curve. This is a greedy approach that gives approximately the same importance to all bits that lie within the same bit plane, and it ensures that the error it introduces is no larger than the prescribed target MSE.

All in all, each  $q$ -th chunk is encoded using  $q + 1$  bits per coefficient, with each first bit storing the sign and the remaining  $q$  bits the following element-wise linear quantization:

$$\mathbf{s}[j] \mapsto \text{round} \left( (2^q - 1) \cdot \frac{\text{abs}(\mathbf{s}[j]) - \text{abs}(\mathbf{s}[i_q])}{\text{abs}(\mathbf{s}[i_{q+1} - 1]) - \text{abs}(\mathbf{s}[i_q])} \right) \quad (8)$$

with  $\text{abs}(\mathbf{s}[i_q])$  and  $\text{abs}(\mathbf{s}[i_{q+1} - 1])$  being the first and last elements of the  $q$ -th chunk. Since the curve  $\mathbf{s}$  is sorted, these coincide with the chunk's minimum and maximum bounds. We save these bounds verbatim. Note that the first chunk  $q = 0$  uses zero quantization bits overall and does not need a sign, since all its elements are simply mapped to 0. We quantize and save all coefficients within each chunk in the order they appeared in the flattened core tensor (not in their order in  $\mathbf{s}$  after sorting by absolute value), so that they can be directly and efficiently set back in place during decompression.

### 4.3 Mask Encoding

The quantization approach discussed above takes care of the sorted coefficients' magnitude but disregards their original position in the flattened core. We encode this crucial information separately and without loss by means of a vector of presence bits  $\mathbf{c}$  (which starts with '0' everywhere) and a set  $\mathcal{M}$  that keeps coefficient positions that have not yet been quantized. The system works as a sieve on these masks, which act as a significance map: newly processed coefficients in each chunk are marked with '1' in  $\mathbf{c}$ . Then  $\mathbf{c}[\mathcal{M}] = \{\mathbf{c}[j] \mid j \in \mathcal{M}\}$  is compressed by RLE and arithmetic coding. Finally, these coefficients are removed from the set  $\mathcal{M}$ . Thus, the bit presence masks that need to be compressed after each chunk become progressively smaller. As an example, suppose that the unsorted flattened core is the sequence of quantized symbols  $\text{abcdefgh}$ , and suppose the first chunk comprises elements  $\text{a}$ ,  $\text{d}$  and  $\text{e}$ . We store this chunk by writing its symbols in that order followed by the presence mask  $\mathbf{c}[\mathcal{M}] = 10011000$ . Then, indices 1, 4 and 5 are popped from  $\mathcal{M}$ . So if the second chunk comprises symbols  $\text{b}$ ,  $\text{f}$  and  $\text{h}$ , it will need the shorter mask  $10101$ .

This chunk partitioning and encoding strategy generalizes both HOSVD truncation [17], [16], [18] and hard thresholding [2]. The latter defines only three kinds of coefficients: the zeroed-out, the quantized, and the single hot-corner. Instead, the proposed method works with a variable number of threshold-defined chunks, each of which is handled in the same way but with an auto-increasing parameter  $q \geq 0$ . Note that the size of the final compressed masks can in principle vary if we either a) choose a FORTRAN-style core flattening (instead of



C-style), or b) permute the input dimensions prior to compression. We found that such variations influence very little the overall compressed file size in practice.

#### 4.4 Factor Quantization

The square factors  $\{\mathbf{U}^{(n)}\}_n$  usually account for a small proportion of the overall non-zero elements compared to the tensor core (except at very low bit rates). We choose to quantize their columns independently, based on the observation that each factor column interacts with exactly one core slice. We quantize the  $j$ -th column of the  $n$ -th factor using a number of bits  $q$  based on the maximal  $q$  value of all its interacting core slice coefficients:

$$q_i^{(n)} = \max_{r_1, \dots, r_N | r_n = i} \{q(r_1, \dots, r_N)\} + k \quad (9)$$

where  $k$  is a constant and  $q(\cdot)$  is a function mapping each core entry to the number of bits it was encoded with (Sec. 4.2). Conservative values of  $k$  are advisable: each column value interacts with an entire core slice, so its error will be significantly propagated. In our experiments we found  $k = 2$  to be the best compromise, and we use this value throughout all measurements.

#### 5 DECOMPRESSION AND POST-PROCESSING

Decompression follows straightforwardly by inverting the steps described above. The core is populated chunk by chunk using arithmetic and run-length decoding plus linear dequantization, the factors are dequantized too, and finally the HOSVD transform is reversed via  $N$  TTM products as in Eq. 3. This is significantly faster than compression (see Sec. 6) since a) no covariance and eigenvalue decomposition are needed; and b) no chunk thresholds need to be selected.

##### Compression-domain Resampling

Thanks to multilinearity, filtering operations on compressed tensors can be efficiently performed via convolution on their factor matrices; see e.g. [28, 29]. Separable filters  $\mathcal{F} = \mathbf{u}^{(1)} \otimes \dots \otimes \mathbf{u}^{(N)}$  are particularly straightforward to apply:

$$\mathcal{T} * \mathcal{F} = \mathcal{B} \times_1 (\mathbf{U}^{(1)} * \mathbf{u}^{(1)}) \times_2 \dots \times_N (\mathbf{U}^{(N)} * \mathbf{u}^{(N)}) \quad (10)$$

where  $\mathbf{U}^{(n)} * \mathbf{u}^{(n)}$  denotes column-wise convolution between a matrix and a vertical vector. In other words, each row of the  $n$ -th factor becomes a linear combination of its neighboring rows, weighted by the vector  $\mathbf{u}^{(n)}$ . This operation has a negligible cost compared to the decompression, which has to be performed anyway for visualization. Following this principle, we have implemented three options for compressed-domain decimation:

- Downsampling: we simply select an evenly spaced subset of the factor rows and discard the rest.
- Box filtering: we average consecutive rows together.
- Separable Lanczos-2: we convolve column-wise the factors with a 1D Lanczos kernel prior to subselection. We use the 3-lobed kernel, i.e. 5 samples with window parameter equal to 2:

$$u(x) = \begin{cases} \text{sinc}(x) \cdot \text{sinc}(x/2) & \text{if } -2 < x < 2 \\ 0 & \text{otherwise} \end{cases}$$

with  $x = \{-2, 1, 0, 1, 2\}$ , where  $\text{sinc}(x) := \frac{\sin(\pi x)}{\pi x}$ .

In our implementation the user can specify index ranges and strides via NumPy-style notation. Immediate applications include previewing, subvolume selection and slicing, reversing dimensions, frame-by-frame visualization in time-dependent data, etc. In all these cases the Tucker core remains unchanged, so the filtering and downsampling asymptotic costs amount to only  $O(NI^2 \log I)$  operations for the column-wise factor convolution where  $I := \max\{I_1, \dots, I_N\}$ .

## 6 RESULTS

We tested the proposed method with 12 integer and floating-point data sets (all details and sources are shown in Tab. 1). Our external libraries are Eigen 3.2.9 for matrix manipulations, products and eigenvalue decompositions (with its `SelfAdjointEigenSolver` class for symmetric real matrices) and ZLIB 1.2.9 for the lossless compression pass. We used a 4-core Intel i7-4810MQ CPU with 2.80GHz and 4GB RAM.

We have measured the compression performance of TTHRESH against three state-of-the-art compressors:

- ZFP [11] (version 0.5.0 as implemented in [34]). We use the fixed accuracy mode (which usually yields the best compression rates) and vary its absolute error tolerance (`-a`).
- SZ [4] (version 1.4.10 as implemented in [35]). We use the relative error bound mode and vary accordingly the relative bound ratio parameter (`relBoundRatio`).
- SQ [6] (our own implementation). We vary the absolute error tolerance and stream the output through the LZMA lossless compressor as advised in the original paper.

All codes were compiled with g++ at maximum optimization (`-O3` flag). Since SZ does not readily support integer data types, we first cast all 8-bit volumes to 64-bit floats; we measure compression ratios w.r.t. the original data for all four compressors. Fig. 4 shows the resulting error curves in terms of PSNR vs. compression ratio over all sample volumes. We observe a recurring pattern from lower to higher compression ratio: our proposed algorithm performs similarly (sometimes worse) than other methods for lower ratios, up to a tipping point after which it is better by a widening margin. Although this point can vary significantly, the general behavior is consistent across all data sets we tested. We argue that the usual rates at which TTHRESH performs best are the most adequate for visualization purposes. To support this claim we present several volume renderings before and after compression at two levels of quality in Fig. 5 as well as in the paper teaser (Fig 1).

We also note that, at medium to high compression ratios, TTHRESH tends to preserve well the coarsest features and smoothen out or eliminate smaller details. See for example Fig. 6 for a sequence of zoomed-in renderings under progressively heavier compression that make this phenomenon evident. It is only at exceedingly high ratios that block-like features start to appear, whereas other algorithms suffer from a much faster visual degradation. This multiscale feature-selective behavior is similar to that observed in truncation-based tensor compression [16]. It is further backed by empirical observation of the Fourier spectra of our compressed data sets. In Fig. 7 we show three example factor matrices for the U volume and their corresponding Fourier transforms along the spatial dimension (i.e. factor columns). Often, each vector in the HOSVD basis corresponds roughly to one frequency wavefunction that has been tuned to better match the specific input data set. As stated earlier, the proposed chunk partitioning and compression (Alg. 1) aims to alter all core coefficients as homogeneously as possible. Since most of these coefficients lie far from the hot corner and thus correspond to high frequencies, we expect the proposed compressor to modify and cancel those frequencies more heavily. This is consistent with what we showed in Fig. 6 where TTHRESH acts as a low-pass filter. To better illustrate this shift towards low frequencies, we depict in Fig. 8 the Fourier magnitude histograms obtained at different compression rates. Note that SZ, SQ and ZFP behave in the opposite way as they rather shift the spectrum towards the right.

Regarding computational speed, we plot in Fig. 9 the compression and decompression times for the smallest data set (the Teapot, 11.1MB) as well as for one of the 512MB ones (the Isotropic-fine). Our method is between 0.5 and 2 orders of magnitude slower than the fastest one, namely ZFP, but compression is generally faster than SQ. It is rather asymmetric as we expected from Sec. 5: the average compression/decompression times for those measurements was 6.7s/1.3s (Teapot) and 147.7/44.2s (Isotropic-fine). Note also that the varying accuracy curves between all four compared algorithms make a fully fair

Table 1. The 12 data sets tested in this paper.

Name	Dimensions	Type	Size	Source
“Foot”, “Engine”	$256 \times 256 \times 256$	8-bit unsigned int	16 MB	The Volume Library [30]
“Teapot”	$256 \times 256 \times 178$	8-bit unsigned int	11.1 MB	The Volume Library [30]
“Isotropic-coarse”, “Isotropic-fine”, “Channel”, “MHD”, “Mixing”	$512 \times 512 \times 512$	32-bit float	512 MB	All available pressure fields from the Johns Hopkins Turbulence Database [1]
“Viscosity”, “Density”	$384 \times 384 \times 256$	64-bit float	288 MB	Lawrence Livermore National Laboratory (Miranda simulation [31])
“U”	$288 \times 192 \times 28$	64-bit float	11.8 MB	National Center for Atmospheric Research (Community Earth System Model [32])
“Jet-u”	$400 \times 250 \times 200$	64-bit float	152.6 MB	Sandia National Laboratories (S3D simulation [33])

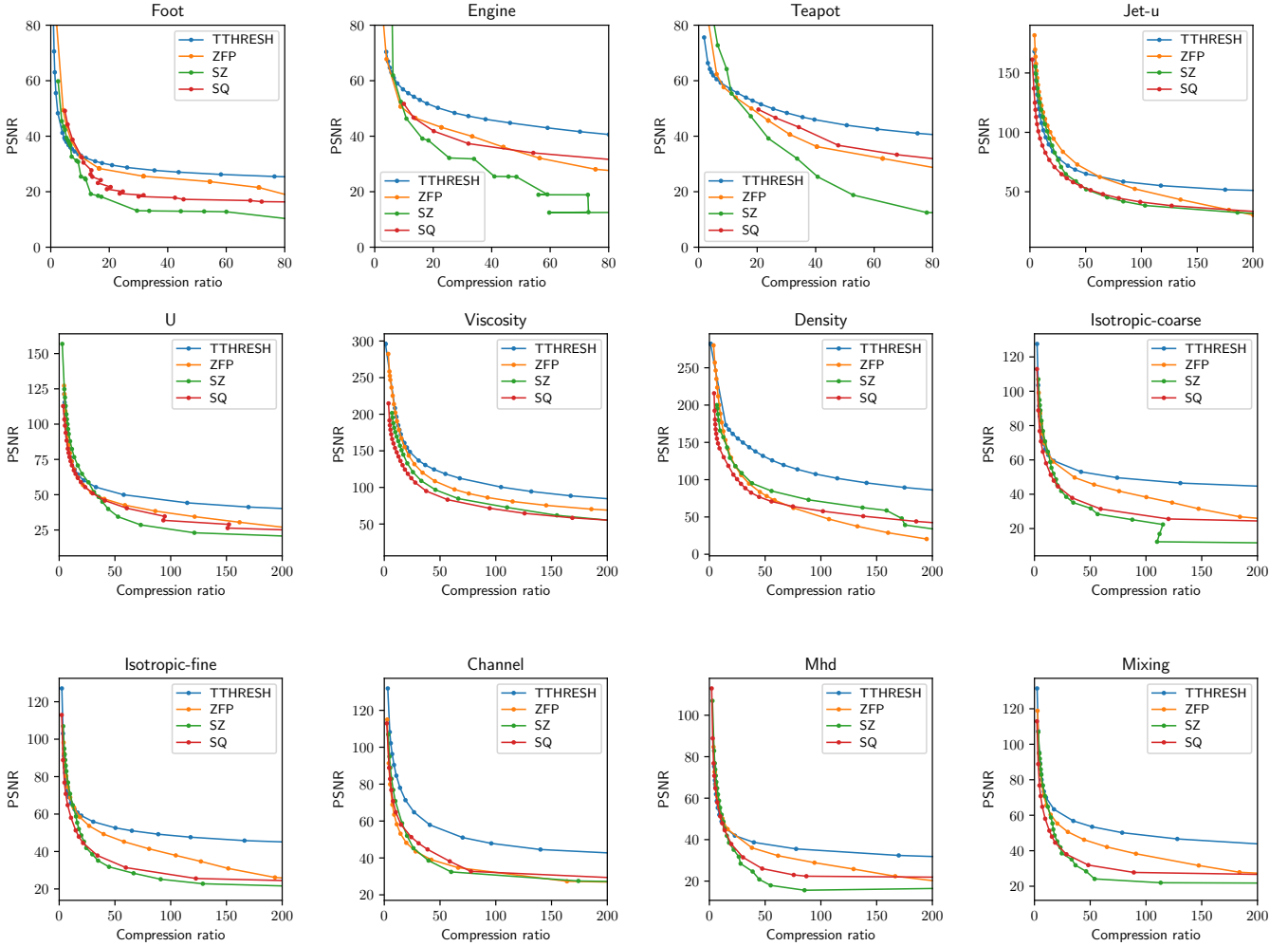


Fig. 4. Compression quality curves (higher is better) for our method compared to SZ, SQ and ZFP over 12 example volumes and varying compression ratios (up to 80:1 for integer data, and 200:1 for floating-point data).

comparison difficult. For consistency with Fig. 4 we did the comparison in terms of time vs. compression ratio, but note that TTHRESH fares better in terms of quality in large parts of the error spectrum.

Our last experiment is reported in Fig. 10, where we demonstrate visual results of decimation along the factor matrices (Sec. 5) followed by decompression. Note the differences between the three methods implemented and the superiority of Lanczos’ kernel for this task.

## 7 DISCUSSION

We observe that the proposed algorithm achieves competitive accuracy at low to medium compression ratios and consistently outperforms other compressors at medium to high ratios; see the higher PSNR curves for our method in the middle to right regions of each plot from Fig. 4. The overtaking point at which TTHRESH surpasses the other algorithms typically produces renderings that are already close to visually indistinguishable to the original data set. This is especially true for higher bit depths. We believe our method is thus a good choice

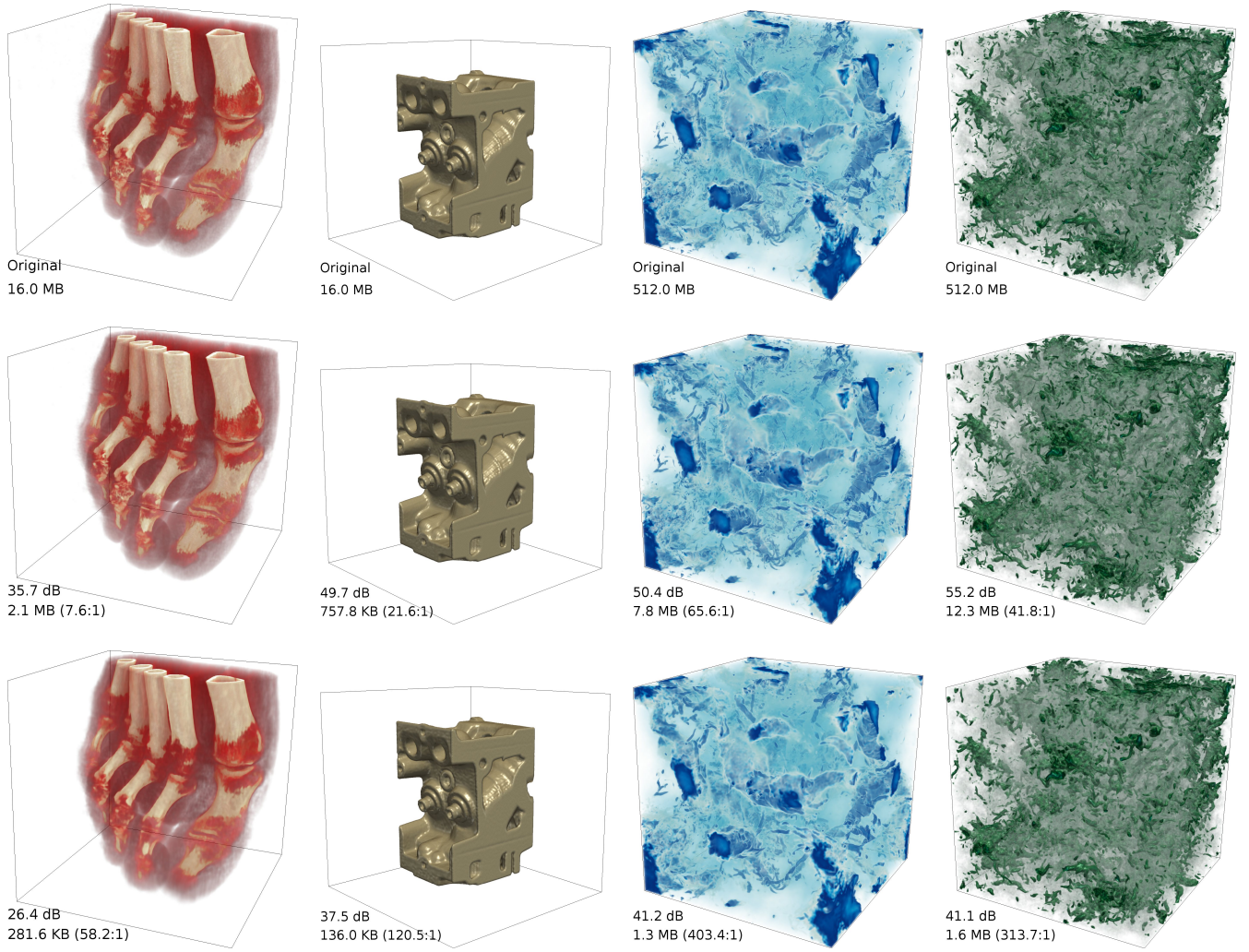


Fig. 5. Four example volumes: the Foot and Engine CT scans (both 8-bit unsigned int), and the Isotropic-coarse and Mixing turbulence simulations (both 32-bit float). Rows from top to bottom: original, higher quality, and lower quality. All these compressed volumes take half or less the space needed with the other two methods tested at equivalent PSNR (except the Foot at higher quality, which performs similarly); see also Fig. 4.

for applications with reasonable error tolerance (chiefly, visualization-related). In addition, we showed how our choice of global bases help the method achieve a very smooth degradation rate. This is manifested both as a Fourier spectrum shift and as a visually parsimonious erosion of the smaller details and features. Since each threshold is chosen on a coefficient by coefficient basis, the range of possible final errors has an extremely fine granularity. Also, the error that arises from the core compression is upper-bounded thanks to careful selection of inter-chunk limits within the coefficient curve. Last, the compressed-domain filtering and resampling features are rather unique strengths of the tensor decomposition framework, only possible thanks to its multilinearity. Any separable filter and resampling can be applied with little cost by manipulating the factors column-wise before the final Tucker reconstruction. This is often much more challenging in other compression methods, especially brick-based and non-transform ones. Even though Lanczos antialiasing results are visually superior when lowering a data set’s resolution, we believe the other decimation methods remain useful for other operations such as region/slice selection, projections, etc.

### Limitations

TTHRESH’s compression rates and smooth degradation come at the price of its monolithic approach to the transform core. This puts it in the slower end of the spectrum of volume compressors, especially compared to those designed for speed such as ZFP. Random-access

decompression is also relatively costly, as one must traverse the whole core in all cases. For example, while progressive transmission is possible in principle (it suffices to send and set in place the rightmost chunks first), a full decompression of each partial core is still required. To tackle these issues one may resort to splitting the data set and using the proposed compressor on a brick-by-brick basis, in the spirit of tensor-compressed multiresolution rendering systems [17, 29].

## 8 CONCLUSION

We have introduced a novel tensor decomposition based compression algorithm with an emphasis on storage/visualization applications whose foremost priority is data reduction at high compression ratios. Unlike previous HOSVD-driven approaches, this reduction is achieved by keeping all ranks followed by quantization with as-fine-as-possible granularity, namely at the transform coefficient level. It is, to the best of our knowledge, the first tensor compressor (and specifically, HOSVD-based) that uses adaptive quantization, also on the factor matrices. The main property we exploited was factor orthogonality, which ensures that all coefficients affect equally the final  $l^2$  error and so allows us to sort the full core as a single block. Our algorithm possesses advantages that are inherent to multilinear transforms in general and tensor decompositions in particular, including support for linear manipulation of the data set in the compressed domain.

We developed TTHRESH focusing primarily on optimizing data re-



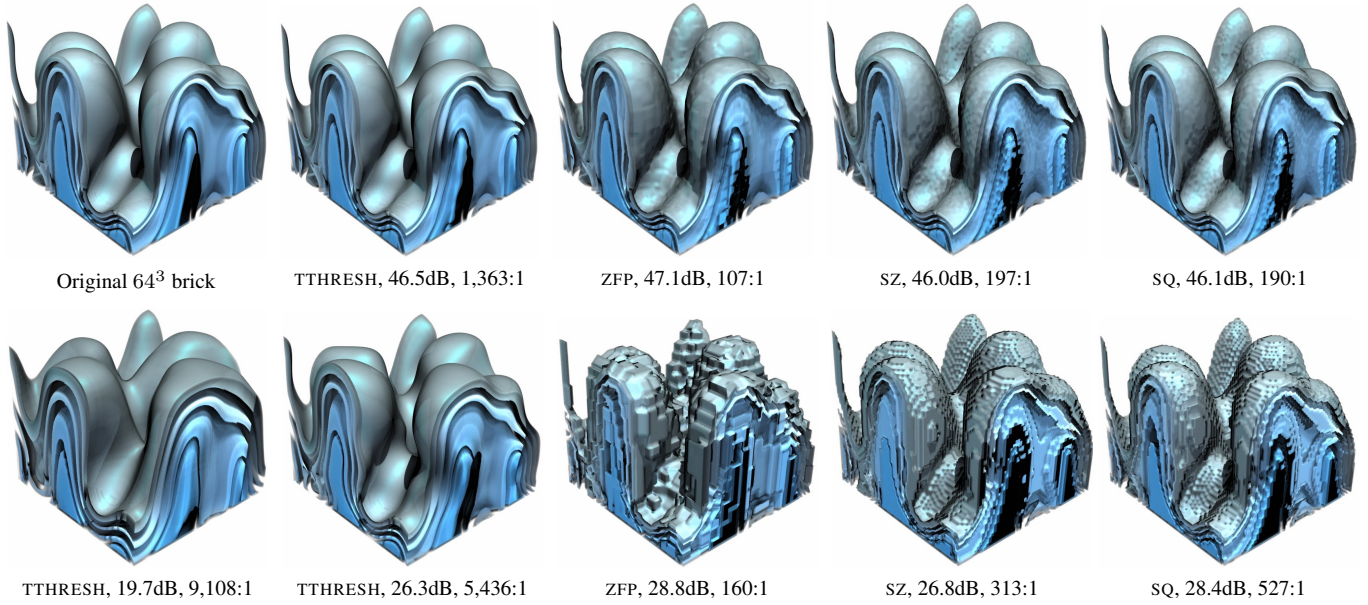


Fig. 6. The HOSVD produces custom data-dependent bases that make the proposed algorithm degrade visually very smoothly up to extreme compression rates. Depicted is a  $64^3$  brick that was cut out from the center of the Density volume after compression with varying quality and algorithms (measurements correspond to the full volume). Unlike other compressors, TTHRESH avoids blocky artifacts; instead, it erodes and merges features at progressively coarser scales.

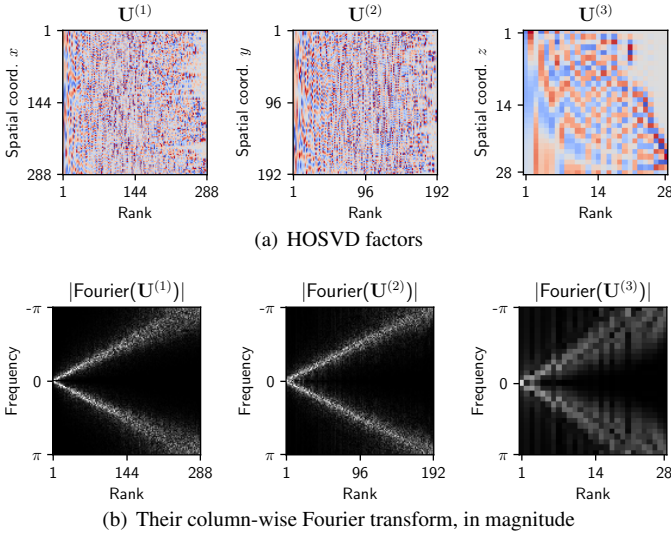


Fig. 7. Factors obtained from the U data set along with their Fourier transform. HOSVD bases often resemble cosine wavefunctions and are rather sparse signals in the frequency domain.

duction rates, and less so on general compression/decompression speed. We have realized that these speeds (especially compression) can be increased significantly at a relatively small accuracy cost in multiple ways, for example by adding a core truncation step during the HOSVD, moderating the eigensolver's number of iterations, or early-stopping the binary search that determines the inter-chunk thresholds. These possibilities will be the subject of future investigation.

#### ACKNOWLEDGMENTS

This work was partially supported by the University of Zurich's Forschungskredit "Candoc", grant number FK-16-012, and partially performed under the auspices of the U.S. Department of Energy by Lawrence Livermore National Laboratory under Contract DE-AC52-

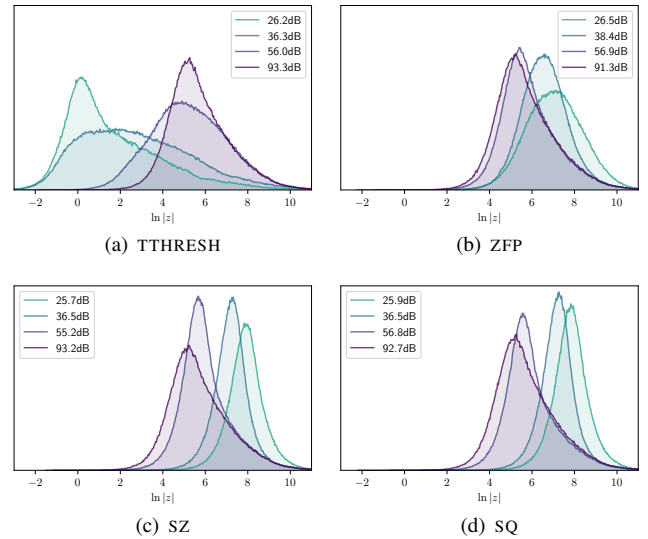


Fig. 8. Logarithmic histograms of the Fourier transform magnitude at different compression quality levels of the U volume. TTHRESH shifts the spectrum towards lower frequencies, as opposed to the other three methods which tend to introduce higher frequencies instead.

07NA27344. The authors wish to thank Stephen Hamilton from Johns Hopkins University as well as the other institutions listed in Tab. 1 for kindly providing the data sets we have used for testing.

#### REFERENCES

- [1] "Johns Hopkins Turbulence Database," <http://turbulence.pha.jhu.edu/newcutout.aspx>.
- [2] R. Ballester-Ripoll and R. Pajarola, "Lossy volume compression using Tucker truncation and thresholding," *The Visual Computer*, pp. 1–14, 2015.
- [3] S. Lakshminarasimhan, N. Shah, S. Ethier, S. Klasky, R. Latham, R. Ross, and N. F. Samatova, "Compressing the incompressible with isabela: In-situ



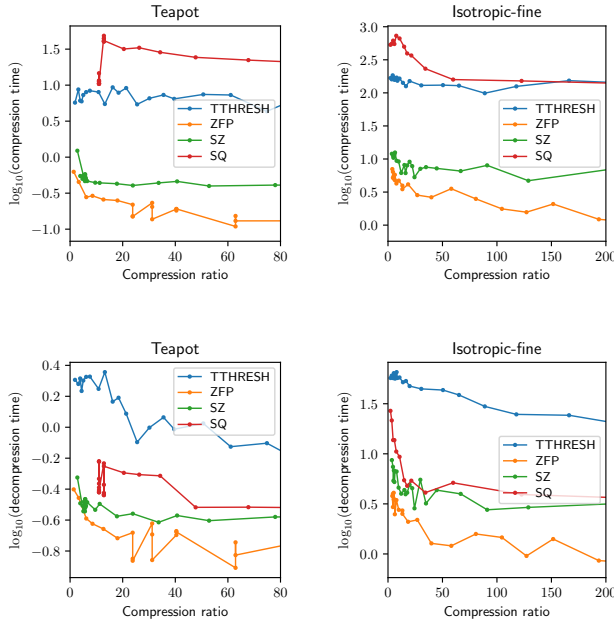


Fig. 9. Compression (top row) and decompression (bottom row) times for two volumes and a range of different compression ratios.

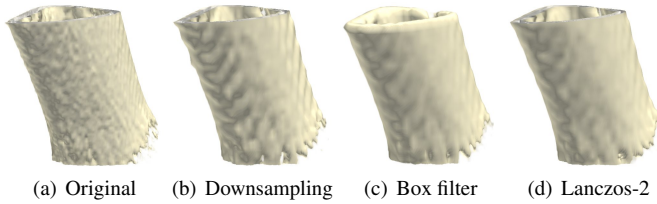


Fig. 10. (a) a  $60^3$  region of the Foot data set. (c-d): 2-fold decimated versions at 7.5:1 compression using the three different methods from Sec. 5. Lanczos minimizes both the blocky aliasing along edges of pure downsampling and the erosion that the box filter incurs (top of the bone).

reduction of spatio-temporal data,” in *Euro-Par Conference on Parallel Processing*, vol. 1, Aug. 2011, pp. 366–379.

- [4] S. Di and F. Cappello, “Fast error-bounded lossy HPC data compression with SZ,” in *International Parallel and Distributed Processing Symposium*, May 2016, pp. 730–739.
- [5] M. Soler, M. Plainchault, B. Conche, and J. Tierny, “Topologically Controlled Lossy Compression,” *ArXiv e-prints*, 2018. [Online]. Available: <https://arxiv.org/abs/1802.02731>
- [6] J. Iverson, C. Kamath, and G. Karypis, “Fast and effective lossy compression algorithms for scientific datasets,” in *Euro-Par Conference on Parallel Processing*, 2012, pp. 843–856.
- [7] E. Gobbetti, J. Iglesias Guitián, and F. Marton, “COVRA: A compression-domain output-sensitive volume rendering architecture based on a sparse representation of voxel blocks,” *Computer Graphics Forum*, vol. 31, no. 3, pp. 1315–1324, 2012.
- [8] S. Guthe and M. Goesele, “Variable length coding for GPU-based direct volume rendering,” in *Vision, Modeling and Visualization*, October 2016.
- [9] M. Balsa Rodríguez, E. Gobbetti, J. A. Iglesias Guitián, M. Makhinya, F. Marton, R. Pajarola, and S. K. Suter, “A survey of compressed GPU direct volume rendering,” *Eurographics State of The Art Report (STAR)*, May 2013.
- [10] J. Clyne, P. Mininni, A. Norton, and M. Rast, “Interactive desktop analysis of high resolution simulations: Application to turbulent plume dynamics and current sheet formation,” *New Journal of Physics*, vol. 9, no. 8, p. 301, 2007.
- [11] P. Lindstrom, “Fixed-rate compressed floating-point arrays,” *IEEE Trans-*

*actions on Visualization and Computer Graphics*, vol. 20, no. 12, pp. 2674–2683, 2014.

- [12] H. Wang and N. Ahuja, “Compact representation of multidimensional data using tensor rank-one decomposition,” in *Proceedings Pattern Recognition Conference*, 2004, pp. 44–47.
- [13] Q. Wu, T. Xia, and Y. Yu, “Hierarchical tensor approximation of multidimensional images,” in *Proceedings IEEE International Conference in Image Processing*, vol. 4, 2007, pp. 49–52.
- [14] Q. Wu, T. Xia, C. Chen, H.-Y. S. Lin, H. Wang, and Y. Yu, “Hierarchical tensor approximation of multidimensional visual data,” *IEEE Transactions on Visualization and Computer Graphics*, vol. 14, no. 1, pp. 186–199, 2008.
- [15] S. K. Suter, C. P. Zollikofer, and R. Pajarola, “Application of tensor approximation to multiscale volume feature representations,” in *Proceedings Vision, Modeling and Visualization*, 2010, pp. 203–210.
- [16] S. K. Suter, J. A. Iglesias Guitián, F. Marton, M. Agus, A. Elsener, C. P. Zollikofer, M. Gopi, E. Gobbetti, and R. Pajarola, “Interactive multiscale tensor reconstruction for multiresolution volume visualization,” *IEEE Transactions on Visualization and Computer Graphics*, vol. 17, no. 12, pp. 2135–2143, 2011.
- [17] S. K. Suter, M. Makhinya, and R. Pajarola, “TAMRESH: Tensor approximation multiresolution hierarchy for interactive volume visualization,” *Computer Graphics Forum*, 2013.
- [18] R. Ballester-Ripoll, S. K. Suter, and R. Pajarola, “Analysis of tensor approximation for compression-domain volume visualization,” *Computers and Graphics*, vol. 47, pp. 34–47, 2015.
- [19] G. Wetzstein, D. Lanman, M. Hirsch, and R. Raskar, “Tensor displays: Compressive light field synthesis using multilayer displays with directional backlighting,” *ACM Transactions on Graphics*, vol. 31, no. 4, pp. 80:1–11, 2012.
- [20] R. Ballester-Ripoll and R. Pajarola, “Tensor decompositions for integral histogram compression and look-up,” *IEEE Transactions on Visualization and Computer Graphics*, vol. PP, pp. 1–12, 2018.
- [21] R. Ruiter and R. Klein, “BTF compression via sparse tensor decomposition,” *Computer Graphics Forum*, vol. 28, no. 4, pp. 1181–1188, 2009.
- [22] Y.-T. Tsai, “Parametric representations and tensor approximation algorithms for real-time data-driven rendering,” Ph.D. dissertation, National Chiao Tung University, May 2009.
- [23] Y.-T. Tsai and Z.-C. Shih, “K-clustered tensor approximation: A sparse multilinear model for real-time rendering,” *ACM Transactions on Graphics*, vol. 31, no. 3, pp. 19:1–19:17, 2012.
- [24] Y.-T. Tsai, “Multiway K-clustered tensor approximation: Toward high-performance photorealistic data-driven rendering,” *ACM Transactions on Graphics*, vol. 34, no. 5, pp. 157:1–15, 2015.
- [25] L. de Lathauwer, B. de Moor, and J. Vandewalle, “On the best rank-1 and rank- $(R_1, R_2, \dots, R_N)$  approximation of higher-order tensors,” *SIAM Journal of Matrix Analysis and Applications*, vol. 21, no. 4, pp. 1324–1342, 2000.
- [26] T. G. Kolda and B. W. Bader, “Tensor decompositions and applications,” *SIAM Review*, vol. 51, no. 3, pp. 455–500, 2009.
- [27] L. R. Tucker, “Some mathematical notes on three-mode factor analysis,” *Psychometrika*, vol. 31, no. 3, pp. 279–311, 1966.
- [28] B. N. Khoromskaia and V. Khoromskaia, “Low rank Tucker-type tensor approximation to classical potentials,” *Central European Journal of Mathematics*, vol. 5, no. 3, pp. 523–550, 2007.
- [29] R. Ballester-Ripoll, D. Steiner, and R. Pajarola, “Multiresolution volume filtering in the tensor compressed domain,” *IEEE Transaction on Visualization and Computer Graphics*, to appear 2018.
- [30] “IAPR-TC18 Data Sets,” [http://www.tc18.org/code\\_data\\_set/3D\\_images.php](http://www.tc18.org/code_data_set/3D_images.php).
- [31] W. H. Cabot and A. W. Cook, “Reynolds number effects on Rayleigh-Taylor instability with possible implications for type Ia supernovae,” *Nature Physics*, vol. 2, pp. 562–568, 2006.
- [32] “Community Earth System Model by the National Center for Atmospheric Research,” <http://www.cesm.ucar.edu/index.html>.
- [33] R. Grout, A. Gruber, C. Yoo, and J. Chen, “Direct numerical simulation of flame stabilization downstream of a transverse fuel jet in cross-flow,” *Proceedings of the Combustion Institute*, vol. 33, no. 1, pp. 1629–1637, 2011.
- [34] “ZFP: Library for compressed numerical arrays,” <https://github.com/LLNL/zfp>.
- [35] “SZ: Error-bounded floating-point data lossy compressor,” <https://github.com/disheng22/SZ>.